# Principle and modelling of Transient Current Technique for interface traps characterization in monolithic pixel detectors obtained by CMOS-compatible wafer bonding

Published by IOP Publishing for Sissa Medialab

Received: *June 1, 2016*
Revised: *July 15, 2016*
Accepted: *July 23, 2016*
Published: *August 23, 2016*

# Principle and modelling of Transient Current Technique for interface traps characterization in monolithic pixel detectors obtained by CMOS-compatible wafer bonding

**J. Bronuzzi,**[a,b,1] **A. Mapelli,**[a] **M. Moll**[a] **and J.M. Sallese**[b]

[a] *EP-DT-DD, European Organization for Nuclear Research, CERN, Geneva 23, CH-1211 Switzerland*
[b] *EDLAB STI GR-IEL, École polytechnique fédérale de Lausanne, EPFL, Route Cantonale, Lausanne, 1015 Switzerland*

*E-mail:* jacopo.bronuzzi@cern.ch

Abstract: In the framework of monolithic silicon radiation detectors, a fabrication process based on a recently developed silicon wafer bonding technique at low temperature was proposed. Ideally, this new process would enable direct bonding of a read-out electronic chip wafer on a highly resistive silicon substrate wafer, which is expected to present many advantages since it would combine high performance IC's with high sensitive ultra-low doped bulk silicon detectors. But electrical properties of the bonded interface are critical for this kind of application since the mobile charges generated by radiation inside the bonded bulk are expected to transit through the interface in order to be collected by the read-out electronics. In this work, we propose to explore and develop a model for the so-called Transient Current Technique (TCT) to identify the presence of deep traps at the bonded interface. For this purpose, we consider a simple PIN diode reversely biased where the ultra-low doped active region of interest is set in full depletion. In a first step, Synopsys Sentaurus TCAD is used to evaluate the soundness of this technique for interface traps characterization such as it may happen in bonded interfaces. Next, an analytical model is developed in details to give a better insight into the physics behind the TCT for interface layers. Further, this can be used as a simple tool to evidence what are the relevant parameters influencing the TCT signal and to set the basis for preliminary characterizations.

Keywords: Detection of defects; Detector modelling and simulations II (electric fields, charge transport, multiplication and induction, pulse formation, electron emission, etc); Models and simulations; Solid state detectors

[1] Corresponding author.



doi:10.1088/1748-0221/11/08/P08016

## Contents



2016 JINST 11 P08016

## 1 Introduction

Semiconductor pixel detectors are commonly used for the detection of radiation in particle physics and imaging applications [1] in particular in the biomedical field [2].

Two main approaches can be followed when manufacturing pixel detectors, the hybrid approach and the monolithic approach (figure 1). Hybrid pixel detectors consist in devices where the sensor matrix and the readout electronics are fabricated on two different substrates and then matched, typically by bump bonding. Monolithic pixel detectors on the other hand integrate the detection sensor and the readout electronics on the same substrate in the same technological process [3]. While monolithic detectors have become standard for the detection of light in consumer applications, the hybrid approach is still the default for pixel detectors in high energy physics [4].

A novel low temperature wafer bonding technology was recently developed [5] and demonstrated for the monolithic integration of two 10 $\mu$m thick silicon layers onto a standard 775 $\mu$m thick Si wafer [6]. The introduction of such a CMOS-compatible wafer bonding process is of great interest for the development of pixel detectors. The approach proposed herein foresees to manufacture monolithic pixel detectors by bonding thinned wafers with this technique.

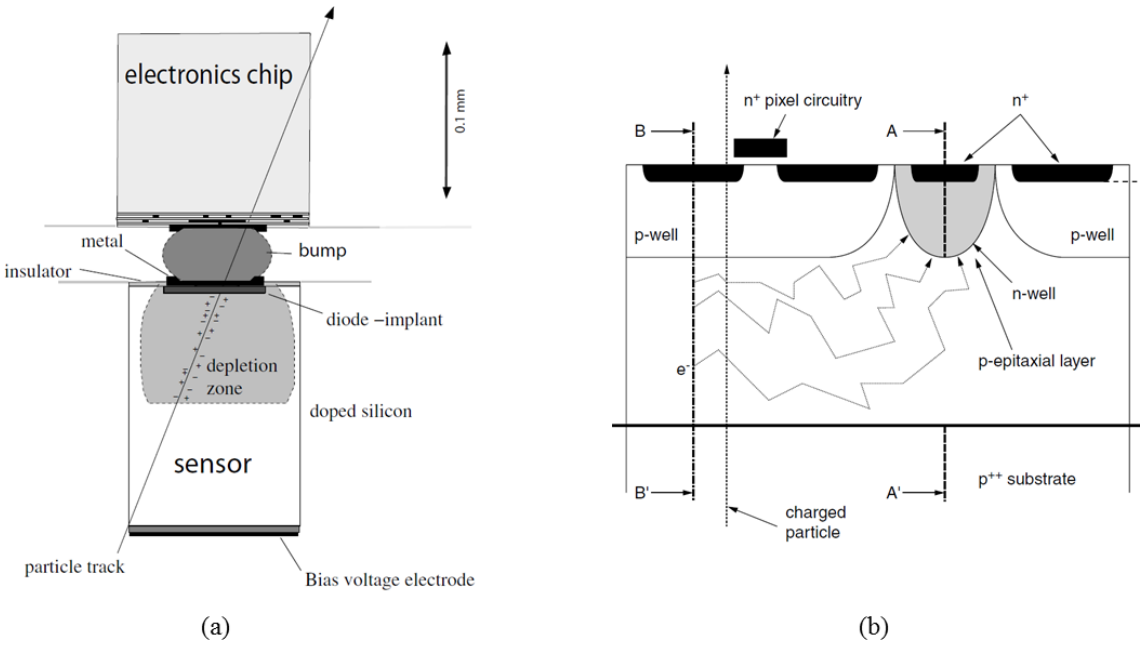


**Figure 1**. Images of: (a) hybrid detector, (b) monolithic detector [3].

The bonding process is performed under vacuum. A first step consists in removing the native oxide to minimize lattice damages in the underlying silicon bulk. Next, bonding is performed by pressing ($0.06\,MPa$) while heating the samples at temperatures between $200°C$ and $300°C$ [5].

However, it has been shown that whatever the experimental conditions an amorphous oxide free layer is generated at the bonded interface [5]. This layer is expected to host crystal defects that may act as deep traps. These could recombine electron-hole pairs and hamper effective collection of carriers generated in the low doped region, far from the interface they have to cross before being collected by the read-out circuit. Electrical properties of the bonded interface are therefore very critical.

Since the bonding process has not been performed yet, no experimental data are currently available. In this context, the aim of this work is to investigate from a merely modelling point of view how the TCT concept, a method widely used for characterization of semiconductor devices and especially for radiation damage in bulk layers [7–10], could also be used for the characterization of the amorphous layer introduced by the bonding process. Before developing the model, we recall what is the principle of the TCT technique (figure 2). This proceeds in two steps. First, free carriers are generated near the surface of the semiconductor layer by absorption of a short light pulse (in our case, at a wavelength of $660nm$, and a pulse length below 100 ps). Next, the photo-generated carriers are drifted away by the applied voltage (that is usually in reverse bias configuration [8]).



2016 JINST 11 P08016

This results in a transient displacement current, which is the output of the signal of interest. An example of the measured output signal obtained with this technique on an NiP diode is shown in figure 2, where, according to the applied bias voltage, holes will move from the generation point near the diode surface toward the counter contact of the diode. In addition, we confirm that the TCAD software Synopsys Sentaurus [11] allows to have good matching between measurements and simulations (observed in figure 2), thus validating the simulation technique that will be used along this work.

As it will be developed in the coming sections, the shape and time dependence of the current is mapping the spatial dependence of the electric field inside the layer, which is itself dependent on the local space charge density distribution. Given that traps present in the semiconductor will affect the space charge profile, and therefore the electric field, the TCT technique happens to be a local probe for the presence of defects inside the bulk.

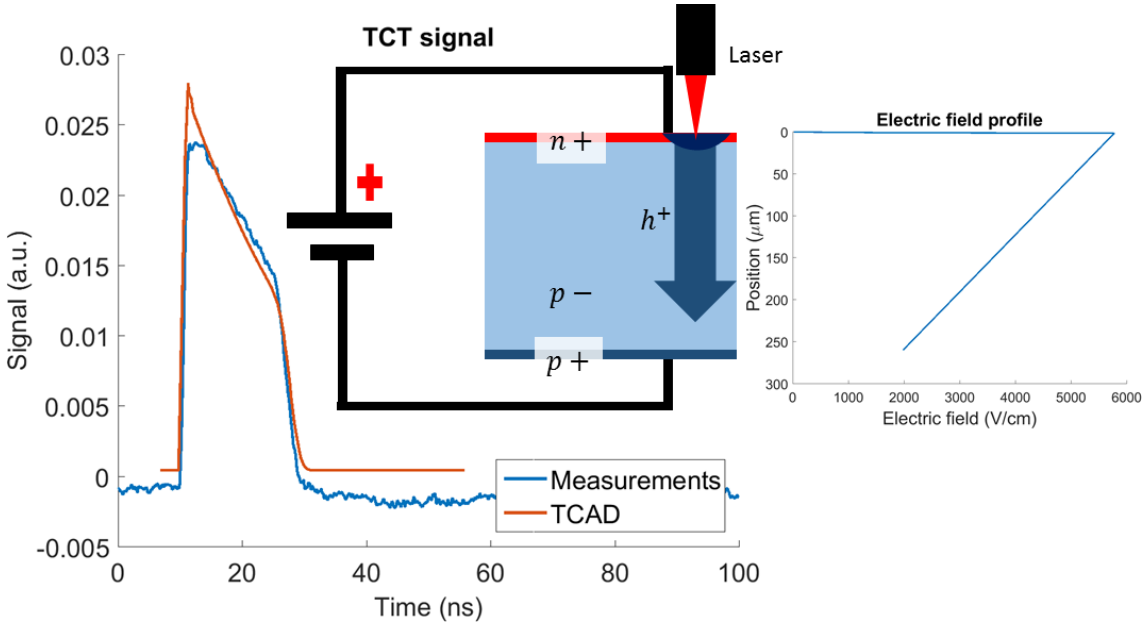


**Figure 2**. Scheme of the TCT measurement and comparison between TCAD simulations and measurements for a non-irradiated (i.e. non-damaged) diode. Electrons and holes are optically generated on the n+ side of a fully depleted diode. Then, considering the applied bias voltage, holes are drifted toward the p+ side of the diode, and a current signal is recorded. In the plot, it is possible to observe a TCT measurement of a PIN diode, with the corresponding TCAD simulated signal.

In case TCT is used for bonding interface characterization, it is worth noticing that this is quite different from bulk defects analysis. Indeed, since the bonding process is expected to create a thin amorphous layer with defects [12], it might be possible that TCT is not able to detect them. Therefore, the goal of this work is to demonstrate that TCT can indeed be used to characterize such thin layers that are deeply embedded in silicon.

For this purpose, first, extensive simulations are done with the TCAD software Synopsys Sentaurus [11] without taking into account the shaping of the signal by the electronics circuit. Even if the TCAD simulations that are considered in this work do not take into account intrinsic RC



2016 JINST 11 P08016

delays inside the circuit, it allows to predict the behaviour of the signal (as in figure 2). Next, an analytical model will be developed and used to understand the physical principles of TCT and use it for fast characterization of future monolithic detectors. To the best of our knowledge, assessment of the TCT technique for interface traps characterization has never been reported so far.

## 2 Assessment of TCT for bonding interface characterization

### 2.1 The idealized structure

The simulated diode structure is shown in figure 3. A PiN structure, with a low doped n-type bulk, has been chosen, since it allows to keep a link with didactic textbooks [13]. The interface with traps is located inside the diode at 50 microns depth. As for the bulk characterization, the diode is reverse biased so that the low-doped silicon layer becomes depleted and carriers injection is performed by illuminating the P-doped side of the diode with a laser pulse in the ps range. Electrons that are generated inside the space charge region of the diode (near the surface) will be transported by the electric field towards the N+ contact. Holes moving in the opposite direction will be collected instantaneously. As predicted by the Ramo's theorem, the current transient signal will be controlled by the motion of electrons in the depleted region (this is a displacement current, i.e. charges generate a current during their displacement even though they are not yet collected by the electrodes).

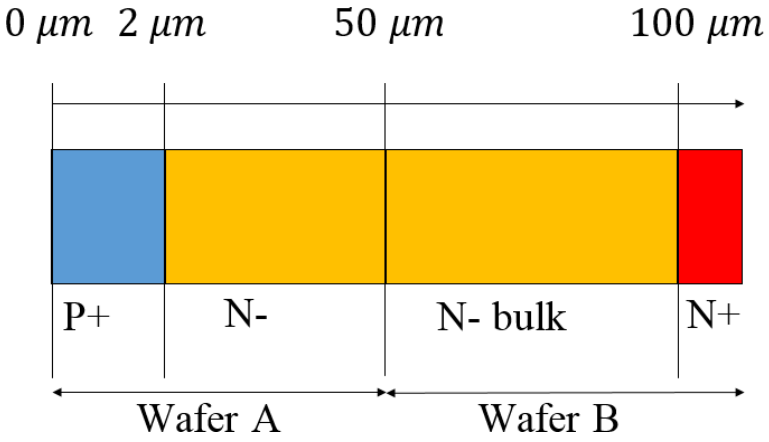


**Figure 3**. Test diode structure. Doping of the P+ region is $2 \times 10^{16}$ cm$^{-3}$ $2 \times 10^{16}$ cm$^{-3}$. Doping of the N- region is $10^{12}$ cm$^{-3}$ $10^{12}$ cm$^{-3}$.

In our example, the bonding interface (black line inside the diode) is located 48$um$ away from the P+N− junction (it is generated by low temperature bonding between the wafer A, that hosts the diode, and the wafer B). Following the characterization done by Flötgen et al. [5], at the bonding interface an amorphous silicon layer of 3$nm$ thickness is expected, without evidence for an oxide layer. In our case, we will model it as a 3$nm$ thick silicon layer with a traps concentration in line with data reported for a-Si. According to Fahrner et al. [12], trap energies are essentially distributed in the midgap of the amorphous silicon. Therefore, we will mainly consider the same energy range, which is also what is reported by other authors [8]. In addition, the concentration of traps inside the amorphous layer will be set to $10^{16}$ cm$^{-3}$ with cross sections of $10^{-14}$ cm$^2$, identical for electrons and holes. These values have been considered based on previous works on traps modelling for



2016 JINST 11 P08016

radiation damaged silicon devices [14]. In literature, traps cross sections range from $10^{-14}\,\mathrm{cm}^2$ and $10^{-16}\,\mathrm{cm}^2$ [8] but no significant differences have been observed for the induced space charge in TCAD simulations using equal cross sections for electrons and holes equal to $10^{-15}\,\mathrm{cm}^2$.

### 2.2 TCAD simulations of TCT in bonded wafers and global assessment of the technique

We first run TCAD simulations of transient currents with picosecond light pulses to estimate the relevance of the technique for interface traps characterization. To this purpose, we analyse the dependence of TCT on physical parameters such as the nature of the traps, their concentration and energy level.

Typical values for TCT parameters are listed in table 1.

**Table 1**. TCT parameters used for the simulations.

| **Parameter name** | **Value** |
|---|---|
| **Temperature** | $253\,K$ |
| **Light wavelength** | $680\,nm$ |
| **Penetration depth (depth at which intensity is 13% of the surface value)** | $9.23\,\mu m$ |
| **Light intensity** | $0.06\,W/cm^2$ |
| **Light pulse time width (Gaussian pulse)** | $50\,ps$ |

A TCAD simulation ran with the parameters listed in table 1 is shown in figure 4. The TCT response subsequent to a light excitation is plotted for a mid-gap acceptor trap $E_t - E_v = 0.55\,\mathrm{eV}$ (where $E_c$ is the conduction band energy level) with a concentration of $3 \times 10^9\,\mathrm{cm}^{-2}$ (that is the equivalent concentration of traps per unit surface inside the thin layer, given by computing the traps volume concentration times the thickness of the traps layer). In addition, since the TCT signal is also sensitive to the reverse voltage on the p-n junction, the reverse bias was also modified.

We note that for a low reverse bias, the current decreases monotonically with time without showing any particular feature. Conversely, when increasing the reverse voltage, a non-monotonic behaviour is observed, which finally turns into a clearly visible peak. This is the signature of an abrupt change of the free carrier velocity inside the depletion region, indicating that the electric field is affected by the space charge in the interface layer. Such a dependence will be explained in more details in the section dealing with the analytical model, but we can safely assert that this supports that the TCT is able to reveal the existence of an anomalous charge density in a very localized region, a premise which was not anticipated before.

Increasing further the reverse voltage moves the peak towards shorter times, which is consistent since the time carriers will spend to reach the counter electrode decreases while increasing their velocity. However, there is an optimum to get the highest peak-to-valley signal in the double peak shape. For instance, when the voltage goes higher than $4V$, this double peak starts to be less visible (see for an applied bias of $6V$ in figure 4).

The influence of the main trap parameters on the TCT signal is now analysed in order to estimate the limits of the technique. Among the critical parameters are the concentration and the energy level of the traps. Changing the traps concentration while keeping the bias voltage to $4V$ (close to optimum value for the present case) and the energy level of the acceptor traps to $E_v + 0.55\,\mathrm{eV}$, the TCT shows a double peak for concentrations higher than $3 \times 10^9\,\mathrm{cm}^{-2}$, see figure 5. However, we



2016 JINST 11 P08016

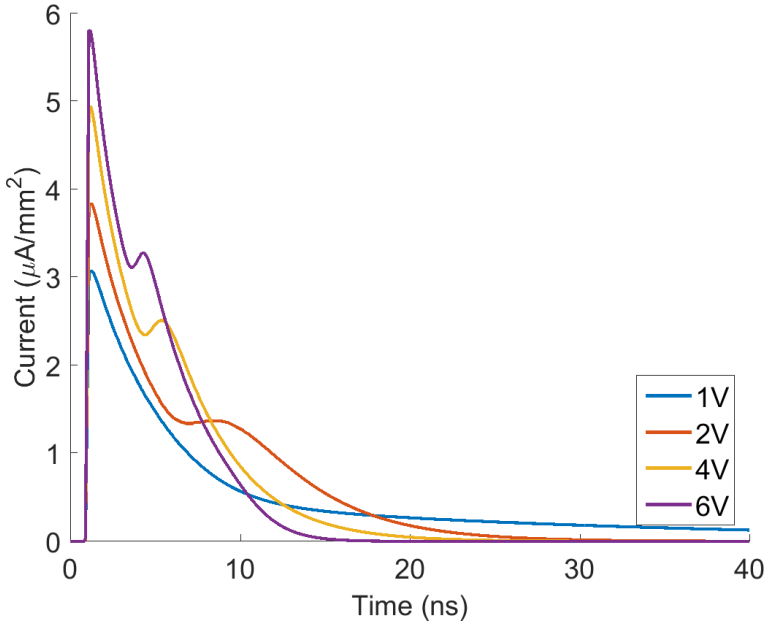


**Figure 4**. Dependence of the TCT signal on the applied voltage. Acceptor traps level $E_v + 0.55\,\text{eV}$, concentration $3 \times 10^9\,\text{cm}^{-2}$.

can already expect that when the trap density is below $3 \times 10^9\,\text{cm}^{-2}$, interface traps characterization might be hardly accessible by TCT. Interestingly such a concentration is in line with typical densities reported by Fahrner et al. [12] in amorphous silicon layers.

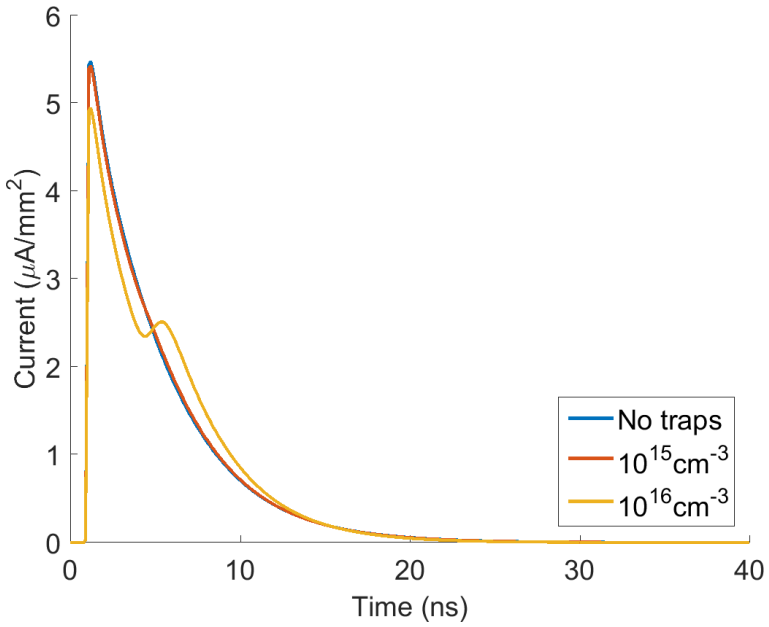


**Figure 5**. Dependence of the TCT signal on the trap concentration inside the interface layer. Acceptor traps level $E_v + 0.55\,\text{eV}$, bias voltage $4V$.

Concerning the nature of traps, i.e. donors or acceptors, we ran simulations still choosing the optimum $4V$ bias together with a trap energy level and a trap concentration of $E_v + 0.55\,\text{eV}$ and $3 \times 10^9 cm^{-2}$ respectively. Figure 6 reveals that the presence of charged donors only does not give

rise to a double current peak. The presence of both acceptor and donor traps (with a concentration equal to $3 \times 10^9$ cm$^{-2}$) will still cause a double peak, but this is less pronounced than for acceptor traps alone.

Conversely, in low doped p-type silicon, it would be donors which would be more 'visible'. The reason for this behaviour will be explained in section 3.4.

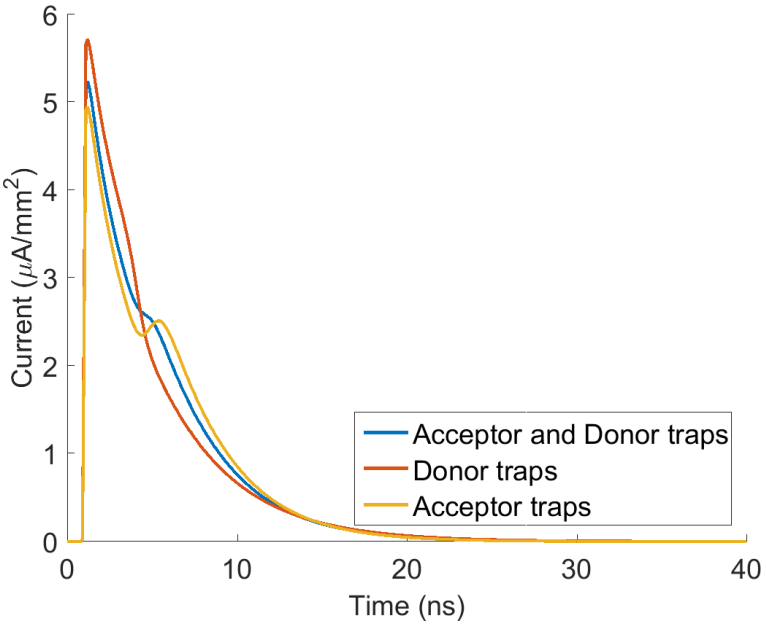


**Figure 6**. Dependence of the TCT signal on the type of traps. Traps level $E_v + 0.55$ eV, concentration $3 \times 10^9$ cm$^{-2}$, bias voltage $4V$.

The last parameter to be investigated is the energy level of the traps. Indeed, TCT is sensitive to the electric field distorted by the presence of charged defects. We have seen that acceptors could modify substantially the TCT signal because these are charged negatively. However, depending on the energy level, traps can have different ionization states. Figure 7 displays the simulated TCT signal for different traps energies (referenced with respect to the valence band) at a bias voltage of $4V$ and with a concentration of $3 \times 10^9$ cm$^{-2}$.

As expected, when the energy level is higher than mid-gap, acceptor traps do not influence the TCT shape, i.e. there is no occurrence of any double peak, the reason being that the level gets less and less occupied with electrons as being shifted towards the conduction band (see section 3.2).

Finally, based on numerical simulations, we can already conclude that the TCT technique can probably be used to estimate the density of mid-gap acceptor traps at a bonding interface of a monolithic detector provided the concentration is higher than $3 \times 10^9$ cm$^{-2}$. Considering donors in the same concentration range, these are still 'transparent' (exhibit a weak signature) and can be better characterized in a p-doped layer (with symmetric configuration with respect to what we used).

An additional information can be extracted from TCT signal shape. Integrating the current with respect to time gives the total collected charge. Comparing this parameter with ($N_t = 3 \times 10^9$ cm$^{-2}$, $E_t = E_v + 0.55$ eV) and without traps we observe that with an applied reverse bias of $4V$, the collected charge is the same and equals $2.48 \times 10^{-14} C$. Therefore, traps present in the interface layer, in the



2016 JINST 11 P08016

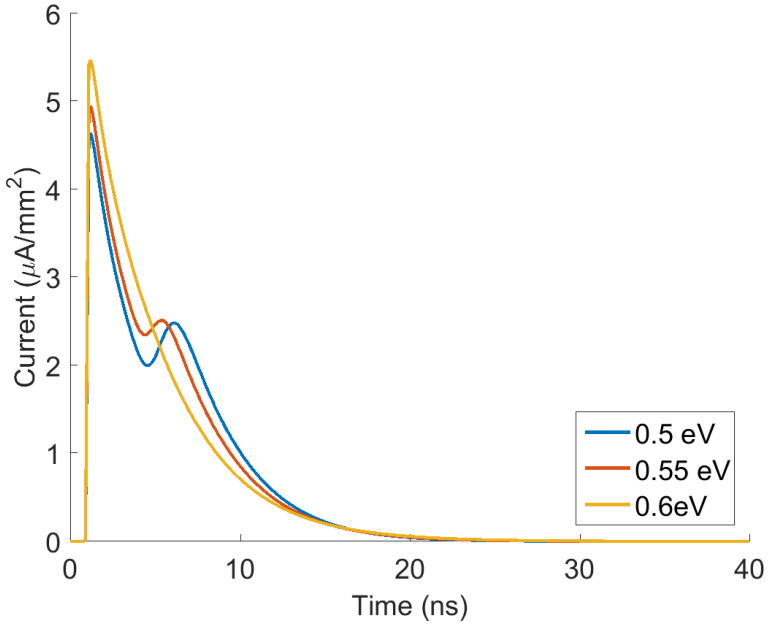


**Figure 7**. Dependence of the TCT signal on the traps energy level. Acceptor traps, concentration $3\times10^9$ cm$^{-2}$, bias voltage $4V$.

investigated parameter range, do not cause detectable trapping of charges that travel through it as far as a high electric field sweeps then out.

In the following, we propose an analytical model for TCT characterization of embedded interface traps.

## 3 Analytical modelling of TCT with interface traps

As already explained, the transient current signal is generated from the displacement of electric charges moving inside the space charge region following Ramo's theorem [15]. In this way, the time dependence of the current and the electric field profile are interrelated. After having validated the principle of the technique for interface characterization by means of numerical simulations, the aim of this section is to develop a full analytical model of TCT to get a detailed understanding of the physical process of TCT and provide a simple tool that can be used to optimize experimental conditions and estimate relevant physical parameters without being forced to perform complex TCAD simulations.

### 3.1 Modelling the electric field distribution

In a first step, we calculate the electric field across the whole structure.

The electric field is obtained by solving the Poisson equation inside and across the different layers of the diode shown in figure 3. We use the same structure as in section 2, to avoid excessive complexity, we assume that the depletion approximation holds. We will see that this restriction is well supported by TCAD numerical simulations.



2016 JINST 11 P08016

Traps are considered to be located at the interface $x_t$ in figure 8. Two different cases have to be analysed whether the space charge region generated by the junction under reverse bias includes or not the interface layer (figures 8a and 8b).

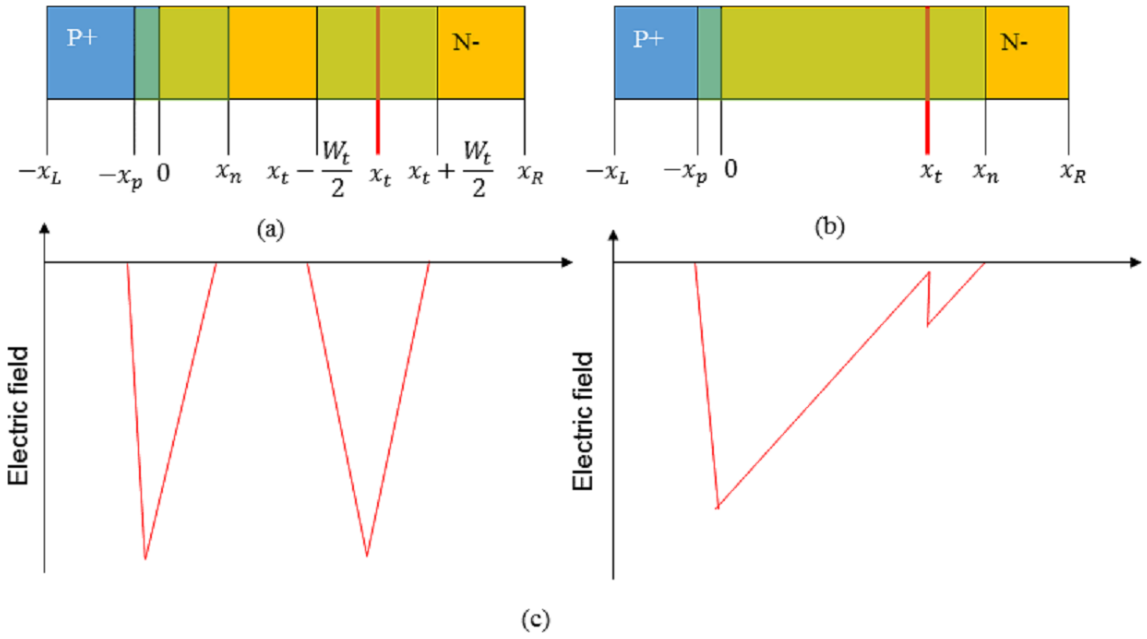


**Figure 8**. Two possible configurations of the space charge region shape (green area) inside the diode: the case where it does not reach the interface layer located at $\mathbf{x_t}$ (a), and the case where it includes the layer (b). The electric field profile is also sketched, in (c).

We identify the different depletion regions where the Poisson equation has to be solved by the black lines in figure 8. The depletion regions edges in the p and n type semiconductor are labelled $x_p$ and $x_n$ respectively, $W_t$ is the total depletion width induced by the traps at thermal equilibrium, $x_t$ is the position of the trap layer and $x_R$ is the back side contact of the diode.

The bias voltage is defined as $V = V_{x_R} - V_{-x_L}$ (where $V_{-x_L}$ is the voltage applied to the P+ side and $V_{x_R}$ is the voltage applied to the N− side).

The boundary conditions used to calculate the electric field in the whole structure are listed hereafter:

- At $-x_L$, the electrostatic potential is equal to $-V$ and the electric field is set to 0.
- The electrostatic potential $\Psi(x)$ must satisfy the semiconductor statistics:

$$V_{\mathrm{bi}} = \frac{k_{\mathrm{b}}T}{q} \ln\left(\frac{N_A N_D}{n_i^2}\right) = \Psi\left(x_n\right) - \Psi\left(-x_p\right) \tag{3.1}$$

  where $V_{\mathrm{bi}}$ is the built in potential, $k_{\mathrm{b}}$ is the Boltzmann constant, $T$ is the temperature, $q$ is the electron charge, $N_A$ is the doping concentration inside the P+ region, $N_D$ is the doping concentration inside the N− region, $n_i$ is the intrinsic carriers concentration.
- In case of two separated space charge regions (figure 8a), the electrostatic potential is assumed symmetric with respect to the interface layer: $\Psi(x_t - W_t/2) = \Psi(x_t + W_t/2)$.



2016 JINST 11 P08016

- The charge density generated by ionized traps inside the interface layer introduces a discontinuity of the electric field:

$$\varepsilon\left(x_t^-\right) - \varepsilon\left(x_t^+\right) = \frac{\left(N_D + N_t\right) q}{\varepsilon} d \tag{3.2}$$

where $\varepsilon\left(x_t^-\right)$ and $\varepsilon\left(x_t^+\right)$ are the electric fields evaluated at $x_t$, $N_t$ is the volume concentration of charged traps (will be modelled further), $\varepsilon$ is the permittivity of Silicon and $d$ is the thickness of the layer with traps [5].

In addition, charge conservation, continuity of the displacement vector (except at the trap interface) and electrostatic potentials are implicitly satisfied. Details of the calculations can be found in appendix A.

Figure 9 shows some cases of electric fields calculated with the analytical model and TCAD simulations for different reverse bias voltages. We can see that the overall profiles obtained by analytical calculations match fairly well those obtained by TCAD simulations.

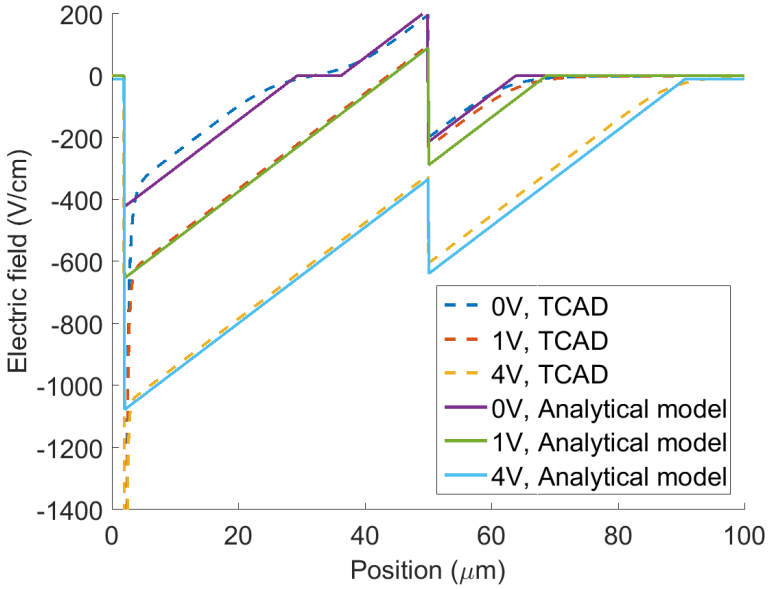


**Figure 9**. Electric field comparison between TCAD simulations and the analytical model. Acceptor traps level $E_v + 0.55\,\text{eV}$, concentration $3 \times 10^9\,\text{cm}^{-2}$.

### 3.2 Modelling interface traps occupancy

To evaluate the electric field, the charge generated from the traps must be evaluated, but the state of these traps depends on the relative position of their energy level with respect to the Fermi level. Basically, traps can be acceptors (positively charged when they capture holes) or donors (negatively charged when they capture electrons) [16].

The general analysis relies on capture and emission rates but this can be quite complex to handle in the dynamic analysis of the structure considered in this work. However, depending on the energy configuration, two asymptotic expressions can be used instead. One applies for traps at equilibrium and the other for traps out of equilibrium, keeping in mind that the status depends on how the diode is operating.



2016 JINST 11 P08016

### 3.2.1 Traps at equilibrium

In case of two separated space charge regions as shown on figure 8a, traps are not subjected to the potential applied to the junction as they are somehow 'isolated' from the applied voltages by adjacent neutral regions. This situation happens when the voltage remains relatively low so that the depletion region generated by traps surrounds the layer at $x_t$. Since traps are in thermal equilibrium, it is possible to use the common relationship for acceptor and donor traps [16] given by:

$$N_{\mathrm{at},e} = N_{\mathrm{at},0}\left(\frac{1}{1 + g\ \exp\left(\frac{E_{\mathrm{at}} - E_{\mathrm{F}}}{k_{\mathrm{b}}T}\right)}\right) \qquad N_{\mathrm{dt},e} = N_{\mathrm{dt},0}\left(\frac{1}{1 + g\ \exp\left(\frac{-E_{\mathrm{dt}} + E_{\mathrm{F}}}{k_{\mathrm{b}}T}\right)}\right) \tag{3.3}$$

where $N_{\mathrm{at},0}$ and $N_{\mathrm{dt},0}$ are the acceptor and donor traps volume concentrations, $N_{\mathrm{at},e}$ and $N_{\mathrm{dt},e}$ are the volume concentrations of charged acceptor and donor traps at thermal equilibrium, $g$ is the degeneracy factor (assumed equal to 1), $E_{\mathrm{at}}$ and $E_{\mathrm{dt}}$ are the acceptor and donor traps energy level, $E_{\mathrm{F}}$ is the Fermi level, $k_{\mathrm{b}}$ is the Boltzmann constant and $T$ is the temperature.

Importantly, once traps are ionized, they modify the potential locally and bend the bands as shown on figure 10. The trap energy level must then include the energy shift self consistently. This is obtained by computing the difference $\Psi_{\mathrm{t},1}\left(x_t\right) - \Psi_{\mathrm{t},1}\left(x_t - \frac{W_t}{2}\right)$ with $W_t$ obtained from appendix A. Adding the bending of the electrostatic potential at the position of the traps $x_t$ to the traps energy level gives finally:

$$E_{\mathrm{at}} = E_{\mathrm{at},0} + \frac{qN_D}{8\varepsilon}\left(\frac{N_D + N_{t,e}}{N_D}d\right)^2 \qquad E_{\mathrm{dt}} = E_{\mathrm{dt},0} + \frac{qN_D}{8\varepsilon}\left(\frac{N_D + N_{t,e}}{N_D}d\right)^2 \tag{3.4}$$

where $E_{\mathrm{at},0}$ and $E_{\mathrm{dt},0}$ are the acceptor and donor traps energy levels referred to the valence band. To conclude, equation (3.5) allows to compute the total volume concentration of charge at equilibrium.

$$N_{t,e} = N_{\mathrm{at},e} - N_{\mathrm{dt},e}\,. \tag{3.5}$$

### 3.2.2 Traps out of equilibrium

When the reverse bias potential increases so that the depletion regions limits $x_n$ and $x_t - W_t/2$ start to overlap, a single depletion region is created such as shown in figure 8b (see appendix for details), also meaning that traps are out of equilibrium. In this case, instead of relations (3.3), one should consider the competition between emission and capture processes to get the ratio between ionized and neutral states, as explained in [17].

Unfortunately, these expressions are not tractable with the analytical model at aim in this work. Then, in order to simplify the analysis, we will identify two cases. The first case assumes that the depletion region $x_n$ goes well beyond $x_t + W_t/2$, which happens for large reverse voltages. Then, it is possible to use the out of equilibrium equations for the traps charge density as given for example from Lutz et al. [18]. In this work, the fraction of charged traps is evaluated assuming a fully depleted semiconductor, which gives:

$$N_{\mathrm{at,oe}} = N_{\mathrm{at},0}\left(\frac{1}{1 + \frac{c_{n,a}}{c_{p,a}}\exp\left(2\frac{E_{\mathrm{at},0} - E_i}{k_{\mathrm{b}}T}\right)}\right) \qquad N_{\mathrm{dt,oe}} = N_{\mathrm{dt},0}\left(\frac{1}{1 + \frac{c_{p,d}}{c_{n,d}}\exp\left(-2\frac{E_{\mathrm{dt},0} - E_i}{k_{\mathrm{b}}T}\right)}\right) \tag{3.6}$$

where $N_{\mathrm{at,oe}}$ and $N_{\mathrm{dt,oe}}$ are the volume concentrations of charged traps out of thermal equilibrium, $E_i$ is the intrinsic Fermi level referenced to the valence band, $c_{n,i}$ and $c_{p,i}$ are the electron and



2016 JINST 11 P08016

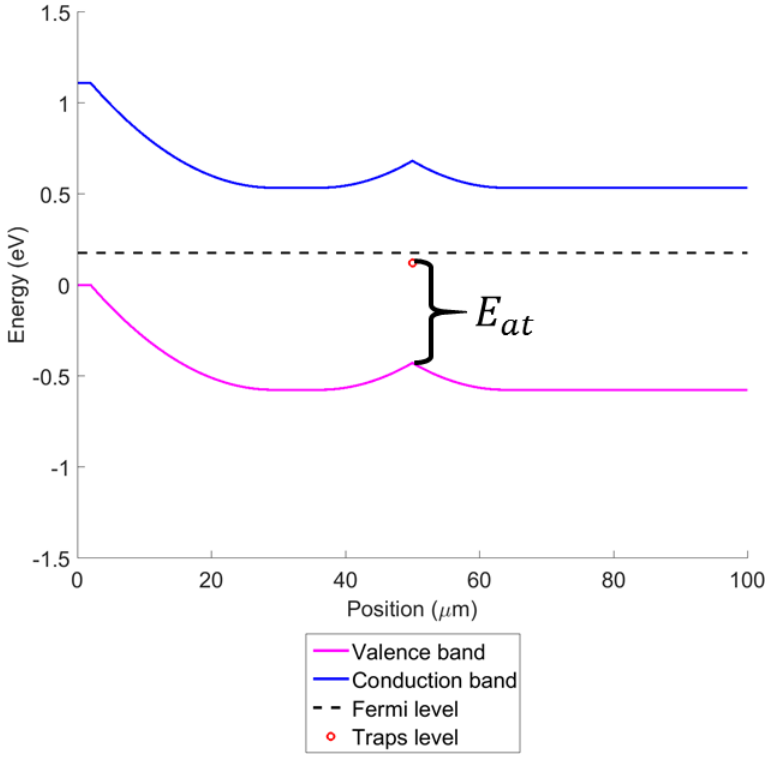


**Figure 10**. Energy band diagram at equilibrium. The band bending affects the traps energy levels reference with respect to the Fermi Level. Acceptor traps level $E_v + 0.6\,\text{eV}$, concentration $3 \times 10^9\ \text{cm}^{-2}$.

hole capture coefficients (subscript $i$ stands for $a$ when referring to acceptors and $d$ to donors). In order to match the occupied fraction of the defects between the TCAD and the analytical model equation (3.6) was used in the following way: it is assumed that the intrinsic level $E_i$ is $E_v + 0.55$ eV. Then the ratio $c_{n,i}/c_{p,i}$ was set to be 0.52 to match the TCAD results on the occupancy of the traps level at $E_v + 0.55$ eV. For all further analytical calculations with different defect energy levels the ratio $c_{n,i}/c_{p,i}$ was fixed to this value. The total volume concentration of charged traps out of equilibrium is then $N_{t,\text{oe}} = N_{\text{at,oe}} - N_{\text{dt,oe}}$.

### 3.2.3 Traps at 'semi-equilibrium'

Between these two extreme situations is the semi-equilibrium condition. This happens for voltages where the depletion regions are still competing against one another in a sense that satisfies the following inequality:

$$x_t - \frac{W_t}{2} < x_n < x_t + \frac{W_t}{2}\,. \tag{3.7}$$

Considering equations (A.2), (A.3) and (A.4) from appendix A and substituting them in (3.7), we obtain the corresponding voltage range for the 'semi-equilibrium' condition:

$$\frac{q}{2\varepsilon}\left(\frac{N_D+N_A}{N_A N_D}\right)\left(N_D x_t - \frac{(N_D+N_{t,e})d}{2}\right)^2 + \frac{2k_\text{b}T}{q} - V_\text{bi} < -V < \frac{q}{2\varepsilon}\left(\frac{N_D+N_A}{N_A N_D}\right)\left(N_D x_t + \frac{(N_D+N_{t,e})d}{2}\right)^2 + \frac{2k_\text{b}T}{q} - V_\text{bi}$$

where $N_{t,e}$ is the concentration of traps at equilibrium.

In this case, there is a competition between 'equilibrium' and 'out of equilibrium' models. To avoid introducing excessive complexity, we propose an empirical definition of a weighting parameter $\omega$ that gives an estimation of the ratio between equilibrium and the out of equilibrium area of the traps depletion region:

$$\omega = \frac{1}{W_t}\left(x_n - \left(x_t - \frac{W_t}{2}\right)\right). \tag{3.8}$$

Relation (3.8) represents the fraction of the depletion region generated by traps calculated when equilibrium is satisfied (region between $\left(x_t - \frac{W_t}{2}\right)$ and $\left(x_t + \frac{W_t}{2}\right)$ in figure 8a, with $W_t$ given in appendix A) which intersects the depletion region that is generated by the voltage applied to the junction, evaluated when there are two depletion regions (whose edge in the n-type silicon bulk is $x_n$, evaluated following equations (A.2) and (A.3)).

Once $\omega$ is computed, the volume concentration of charged traps $N_t$ is evaluated from equation (3.9).

$$N_t = \omega N_{t,\mathrm{oe}} + [1-\omega]\, N_{t,e}\,. \tag{3.9}$$

Obviously, $N_t$ reverts to $N_{t,\mathrm{oe}}$ for a full out of equilibrium condition, i.e. when $x_n > x_t + \frac{W_t}{2}$. Considering different traps concentrations, energy levels and types, we see that there is a good matching between the charged traps concentrations obtained from the model and from TCAD simulations, see table 2 (evaluations are done for two different applied voltages, 1V and $4V$, and traps concentrations are evaluated as surface concentration, equal to $d * N_t$). Moreover, in figure 9 it is possible to observe the matching in the three different regimes, i.e. equilibrium (at $0V$), partially out of equilibrium (at $1V$) and fully out of equilibrium (at $4V$).

In all these situations, the model agrees pretty well with a full numerical treatment.

Having validated this electrostatic approach, we propose to address the modelling of TCT as such.

**Table 2**. Charged Traps concentration from TCAD simulations and the analytical model for voltages of 1V and 4V.

| **Traps type** | **Traps energy level with respect to the valence band ( eV)** | **Voltage applied (V)** | **Charged traps concentration from TCAD ($cm^{-2}$)** | **Charged traps concentration from analytical model ($cm^{-2}$)** |
|---|---|---|---|---|
| **Acceptor** | 0.5 | 1 | $1.6 \times 10^8$ | $1.8 \times 10^8$ |
| **Acceptor** | 0.55 | 1 | $3.0 \times 10^9$ | $2.8 \times 10^9$ |
| **Acceptor** | 0.6 | 1 | $2.5 \times 10^9$ | $2.1 \times 10^9$ |
| **Donor** | 0.55 | 1 | $\sim 0$ | $3 \times 10^5$ |
| **Acceptor** | 0.5 | 4 | $3.0 \times 10^9$ | $3.0 \times 10^9$ |
| **Acceptor** | 0.55 | 4 | $2.0 \times 10^9$ | $2.0 \times 10^9$ |
| **Acceptor** | 0.6 | 4 | $5.8 \times 10^7$ | $5.8 \times 10^7$ |
| **Donor** | 0.55 | 4 | $1.0 \times 10^9$ | $1.0 \times 10^9$ |



2016 JINST 11 P08016

### 3.3 Modelling the transient current

The link between the transient current and the electric field profile is provided by the Ramo's theorem which states that the current generated by a travelling charge inside a parallel plate capacitor is given by:

$$I = \frac{Qv}{L} \tag{3.10}$$

where $Q$ is the charge moving at speed $v$, and $L$ is the distance between the capacitor electrodes. In the case of our diode, electrodes are substituted by the edges of the space charge region. Therefore, since the electron velocity depends on the electric field following the law $v{=}\mu_e\varepsilon$, for each moving electron, the related transient current will be proportional to the electric field evaluated where the electron is at time $t$, i.e. $r\,(t)$.

In addition, we also introduce the field mobility dependence based on the extended Canali model [19]:

$$\mu_e = \frac{\mu_{e,0}}{1+\frac{\mu_{e,0}|\varepsilon(r)|}{v_{\text{sat}}}}$$

where $\varepsilon\,(r)$ is the electric field, $\mu_{e,0}$ is the low field electron mobility ($1417 cm^2/Vs$ for silicon), and $v_{\text{sat}} = v_{\text{sat},0}\left(\frac{300K}{T}\right)^{0.87}$ is the saturation velocity ($v_{\text{sat},0} = 1.07\times10^7 cm/s$).

Considering that $v{=}\mu_e\varepsilon$, we obtain a differential equation in terms of position $r\,(t)$ and time

$$\frac{dr}{dt}{=}\mu_e\varepsilon\,(r)\,. \tag{3.11}$$

Equation (3.11) is then evaluated in each region of figures 8a or 8b using the correct expression for the electric field. Details of the developments are shown in appendix B.

#### 3.3.1 The single charge picture

The TCT signal of a localized charge travelling across the structure choosing a trap energy level of $E_v + 0.5\,\text{eV}$ with a concentration $3\times10^9\,\text{cm}^{-2}$ and at a bias of $4V$ is analyzed first and shown in figure 11.

We notice that the time dependence of the overall TCT signal is reasonably well reproduced between the analytical model and TCAD simulations, meaning that in essence the modelling approach and the principle behind it is correct. However, looking into the details reveals a quite different shape. We will argue that this is attributed to the 'self diffusion' of the initial 'bunch of carriers' as time passes. Indeed, a rough estimation of the diffusion length gives about $5\mu m$ after $10ns$ (in line with travelling times) considering an average mobility of $0.1 m^2/Vs$, thus revealing that during their motion, the initial shape will extend over a non-negligible region in regard to the dimensions of the depletion region.

Without entering into the details, it is possible to obtain the exact solution of the continuity equation with a linearly dependent electric field. However, this requires numerical computations, and therefore an explicit analytical solution cannot be obtained.

#### 3.3.2 The Gaussian approximation of the travelling carrier density

We have seen that the sharp signal predicted by the model is still quite crude and cannot reproduce precisely the shape of numerical simulations. To this purpose, we propose to include a diffusion



2016 JINST 11 P08016

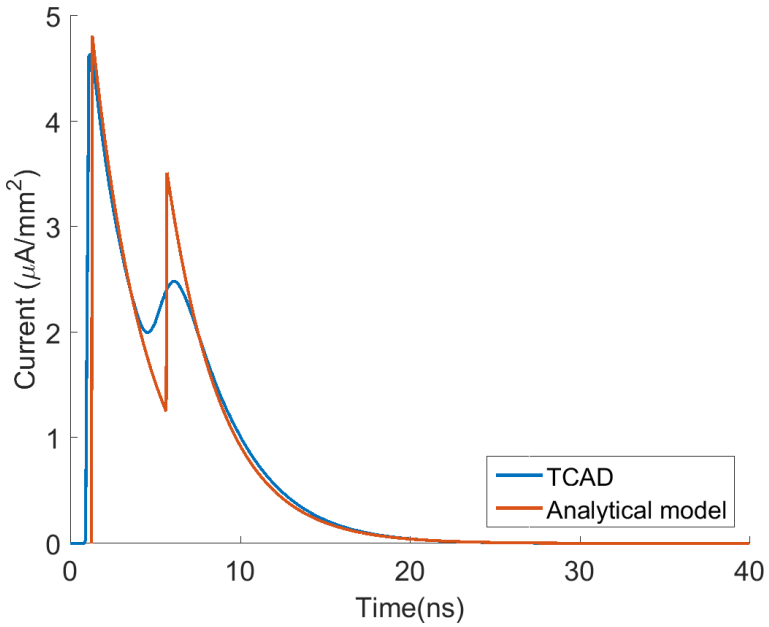


**Figure 11**. TCT signal prediction between TCAD simulations and analytical model simulations. Here a localized charge traveling across the structure is considered. Acceptor traps level $E_v + 0.5$ eV , concentration $3 \times 10^9$ cm$^{-2}$, bias voltage $4V$.

process by introducing a Gaussian function which centre moves according to the mean value of the electric field:

$$n\left(x,t\right) = \frac{N}{\sqrt{4\pi D_n t}} * \exp\left(-\frac{\left(x - r\left(t\right)\right)^2}{4D_n t}\right). \tag{3.12}$$

It is worth noticing that relation (3.12) still represents the solution of the continuity equation in a uniform electric field [20]. However, in our case, the electric field is non uniform and therefore relation (3.12) is merely an approximate solution. The Gaussian has the following features: the maximum equals the number of photo generated electrons $N$, the center is still given by $r\left(t\right)$ that satisfies relation (3.11), and the variance changes with time following the diffusion law with $D_n$ being the diffusion constant.

The transient current density can therefore be defined by the following equation:

$$I\left(t\right) = \beta \int\limits_{\substack{\text{Depletion}\\ \text{region}}} n(x,t)v(x)dx = \beta \int\limits_{\substack{\text{Depletion}\\ \text{region}}} n(x,t)\varepsilon(x)\mu_e(\varepsilon(x))dx \tag{3.13}$$

where $\beta$ is a scaling geometrical parameter defined to match the TCAD current density absolute value. Next, integrals needs to be solved for each region of the diode, in case of two separated space charge regions or a single space charge region, as already done to get the solutions of equation (3.11).

Figure 12a illustrates the new TCT prediction given by the analytical model with the diffusion process included.

It comes out that the approximate analytical model is able to reproduce in many details the dependence of the TCT signal on traps characteristics and applied voltages. For instance, from the evaluation of $x_p$ (equation (A.6)), it is possible to predict that the higher the applied voltage,

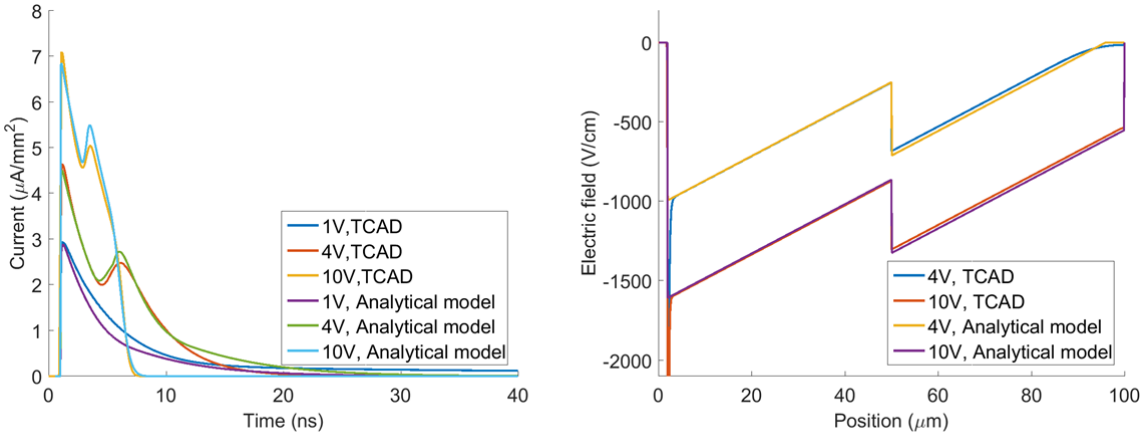


(a) (b)

**Figure 12**. TCAD and analytical model simulations of TCT signal (a) and electric field shape (b) under different biases. Acceptor traps level $E_v + 0.5\,\text{eV}$ , concentration $3 \times 10^9\,\text{cm}^{-2}$.

the larger will be the absolute value of $x_p$ and $x_n$ (equation (A.5)). At some point the electric field will be high enough to drag carriers across the interface that generate a current that will mimic the electric field discontinuity. The dependence of the TCT signal on the trap density is also included since the discontinuity of the electric field at $x_t$ is also related to traps density through equation (3.2). Another interesting information can be obtained from the analytical solution with the diffusion included. Indeed, it is possible to see that, after a certain voltage, the tail of the current is no more visible. This is due to the fact that, when the diode is fully depleted, the electric field is never negligible inside the diode. Therefore, electrons will be rapidly collected by drift, and diffusion will not affect the signal shape.

For lower voltages, there exists a region beyond which the electric field is almost zero. Therefore, once the electron cloud reaches this position, carriers will be collected mainly by diffusion, thus increasing the collection time. In figure 12, it is possible to observe the current shape at 10V (fully depleted diode, figure 12a), and the electric field shapes at 4V and 10V (figure 12b).

### 3.4 Dependence on the nature of the traps

A comment on the influence of the type of traps on the TCT signal is needed. In case of n-type doped silicon bulk, the sign of the discontinuity at the interface needs to be positive (considering the notation in equation (3.2)) in order to have a double peak in the electric field profile (that will cause a double peak in the TCT signal). This happens when charged acceptors are present in higher concentration than charged donors, as they introduce a net negative charge at the interface layer (that in the notation used in this work corresponds to a positive value of $N_t$). Conversely, the presence of donors causes a double peak shape of the transient current when the bulk is lightly p-type doped (and therefore, the doping profile of the testing diode is opposite with respect to the one presented in figure 3). This is due to the fact that they will introduce a positive charge inside a bulk where, when depleted, is negative, resulting in a discontinuity of the electric field. This will give rise to a double peak shape of the electric field, and then of the transient current.



2016 JINST 11 P08016

By looking at equations (3.3) for traps at equilibrium and (3.6) for traps out of equilibrium, it is possible to deduce that, generally speaking, when acceptor traps have an energy level below the band mid gap, they will be charged, while donors will behave in the opposite way. Therefore, double peak will be observed in cases where acceptors energy levels are below mid gap when the diode doping profile is as in figure 3, and donors energy levels are above mid gap when the diode doping profile is opposite to the one presented in figure 3.

## 4 Extraction of charged traps concentration inside the interface layer

Once the transient current signals are obtained for several voltages, we can extract the voltage corresponding to the full depletion of the diode [21]. From figure 12a we observe that the higher the voltage, the shorter (in time) the transient current due to the increase in the electric field and thus in carrier velocity.

For voltages greater than the 'full depletion' value, the diffusion process will become less relevant since the electric field spreads over the whole diode (see the difference between 4V and 10V in figure 12b). At this particular voltage (which can be estimated from the electric field distribution inside the diode using the model), we can evaluate the time needed by the center of the electrons cloud to reach the end of the diode using equation (4.1). This condition is recovered from equation (B.10), where $x_t$ is replaced with $x_{\text{end}}$, that is the value of the thickness of the n-type doped bulk.

$$t_{\text{end}} = \frac{-x_{\text{end}} + \frac{N_A}{N_D} x_p + E_1 \ln\left(-x_{\text{end}} + \frac{N_A}{N_D} x_p\right) - K_1}{-v_{\text{sat}}} . \tag{4.1}$$

When evaluating for example $t_{\text{end}}$ at $V = 4V$ (according to the model, this is close to the full depletion of 4.8V for acceptor traps concentration equal to $3 \times 10^9\,\text{cm}^{-2}$ and an energy level equal to $E_v + 0.5\,\text{eV}$), we find $11.3\,ns$. For voltages higher than this value, the current becomes negligible when $t>t_{\text{end}}$, while this will not happen for lower voltages since the diffusion current is still important for not fully depleted diodes. Then, integrating the signal up to $t_{\text{end}}$, the integral will remain constant above a certain voltage as the current will be negligible for $t>t_{\text{end}}$ (all carriers will have been collected).

However, when performing experiments, the integration time discussed above is an indication, but its value should be fine-tuned according to the measurements. In our case this would be about $10\,ns$. Results for the integral are shown in figure 13.

It is visible that above depletion the current integral starts to exhibit a plateau, same result obtained for example by Bates and Moll [21]. In an experiment, one could try to extract the voltage at which the plateau is reached as indicated by the lines in figure 13. While the saturation value (horizontal line) is clearly defined, the second tangent is difficult to determine due to the shape of the curve. We have extracted a range of possible voltages for the intercept between $V_{\text{fd}} = 4.75V$ and $V_{\text{fd}} = 5.85V$ (the voltage range is indicated by the vertical dashed lines in figure 13). From these voltages, the total charge density inside the volume can be calculated by using equation (A.10). Indeed, considering $x_n = x_R$ and $V = V_{\text{full depletion}}$ at full depletion, the only unknown is the volume concentration of the traps $N_t$ (or the surface concentration $N_t * d$ with $d = 3nm$).



2016 JINST 11 P08016

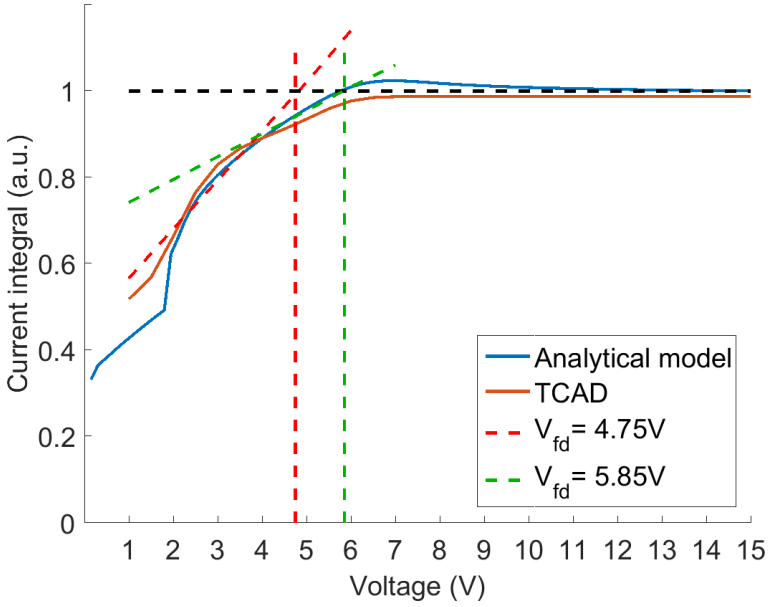


**Figure 13**. TCAD and analytical model simulations of the normalized integral of the TCT current signals at different voltages. Acceptor traps level $\boldsymbol{E_v + 0.5\,eV}$, concentration $\boldsymbol{3 \times 10^9\ cm^{-2}}$.

We obtain respectively $N_t * d = 2.78 \times 10^9$ cm$^{-2}$ (for $V_{\mathrm{fd}} = 4.75V$) and $N_t * d = 1.30 \times 10^9$ cm$^{-2}$ (for $V_{\mathrm{fd}} = 5.85V$), while the charged traps surface concentration is $3 \times 10^9$ cm$^{-2}$ (since acceptor traps with the energy level equal to $E_v + 0.5$ eV are fully ionized).

Therefore, using TCT data, the method allows estimating the charged traps concentration, while fitting the TCAD or analytical model to the obtained transient data will give a much more precise value for the charge stored in the interface.

## 5 Conclusion

In this paper, a new characterization method for bonded interfaces with deep traps is investigated by means of numerical and analytical simulations of photo generated transient currents, the so-called TCT. It comes out that this technique is likely to be used to analyse the presence of traps inside ultra-thin interface layers in wafer bonded monolithic detectors, and possibly in a variety of semiconductor heterostructures that can be fabricated with the promising low temperature wafer bonding technology. This preliminary work focused on the principle of the TCT and highlighted what are the key technological parameters that can be assessed with this technique. In particular, the total charge density inside the device. To this purpose, we proposed a physics based model that helps understanding fine points of TCT for this projected application and understand what are the most relevant physical parameters of the interface layer that can be acquired, like traps concentration, type and energy level. Besides, it seems that injected charges can still be collected through the interface without being captured if reasonable interface trap densities and energy levels are used and an electric field is applied.



2016 JINST 11 P08016

# A Solution of the Poisson equation

In the following appendix, the equations for variables and constants from the solution of the Poisson equation in the cases explained in the Electrostatic modelling section, are shown, for each diode region.

## A.1 Two space charge regions case

- **Region $P+$, $n$ $-x_L < x < -x_p$**: in this region, silicon is not depleted, and therefore the equations will be:
  - $\varepsilon_{P+,n}(x) = 0$;
  - $\Psi_{P+,n}(x) = -V$.
- **Region $P+$ $-x_p < x < 0$**: in this region, silicon is depleted, and therefore, by solving the Poisson equations:
  - $\varepsilon_{\mathrm{P+}}(x) = -\frac{N_A q}{\varepsilon}(x + x_p)$;
  - $\Psi_{\mathrm{P+}}(x) = \frac{N_A q}{2\varepsilon}\left(x + x_p\right)^2 - V$.
- **Region 1** $0 < x < x_n$: also in this region silicon is depleted, and therefore:
  - $\varepsilon_1(x) = \frac{N_D q}{\varepsilon}x - \frac{N_A q}{\varepsilon}x_p$;
  - $\Psi_1(x) = -\frac{N_D q}{2\varepsilon}x^2 + \frac{N_A q}{\varepsilon}x_p x + \frac{N_A q}{2\varepsilon}x_p^2 - V$.
- **Region 2** $x_n < x < x_t - \frac{W_t}{2}$: Si is not depleted:
  - $\varepsilon_2(x) = 0$;
  - $\Psi_2(x) = -\frac{N_D q}{2\varepsilon}x_n^2 + \frac{N_A q}{\varepsilon}x_p x_n + \frac{N_A q}{2\varepsilon}x_p^2 - V$.
- **Region $t$, 1** $x_t - \frac{W_t}{2} < x < x_t$: Si is depleted, in this case by the charge generated by traps:
  - $\varepsilon_{t,1}(x) = \frac{N_D q}{\varepsilon}\left(x - x_t + \frac{W_t}{2}\right)$;
  - $\Psi_{t,1}(x) = -\frac{N_D q}{2\varepsilon}\left[x^2 + x_n^2 + \left(x_t - \frac{W_t}{2}\right)^2\right] + \frac{N_D q}{\varepsilon}\left(x_t - \frac{W_t}{2}\right)x + \frac{N_A q}{\varepsilon}x_p x_n + \frac{N_A q}{2\varepsilon}x_p^2 - V$.
- **Region $t$, 2** $x_t < x < x_t + \frac{W_t}{2}$:
  - $\varepsilon_{t,2}(x) = \frac{N_D q}{\varepsilon}\left(x + \frac{W_t}{2} - x_t\right) - \frac{(N_D+N_t)d}{\varepsilon}q$;
  - $$\Psi_{t,2}(x) = -\frac{N_D q}{2\varepsilon}\left(x+\frac{W_t}{2}-x_t\right)^2 + \frac{(N_D+N_t)d}{\varepsilon}q(x-x_t) + \frac{N_D q}{2\varepsilon}\left(\frac{W_t}{2}\right)^2 - \frac{N_D q}{2\varepsilon}\left[x_t^2+x_n^2+\left(x_t-\frac{W_t}{2}\right)^2\right] + \frac{N_D q}{\varepsilon}\left(x_t-\frac{W_t}{2}\right)x_t + \frac{N_A q}{\varepsilon}x_p x_n + \frac{N_A q}{2\varepsilon}x_p^2 - V.$$

- **Region $N-$, $x_t + \frac{W_t}{2} < x < x_R$**: Silicon is not depleted:
  - $\varepsilon_{N-}(x) = 0$;
  - $\Psi_{N-}(x) = -\frac{N_D q}{2\varepsilon} W_t^2 + \frac{(N_D + N_t)\, d}{\varepsilon} q \frac{W_t}{2} + \frac{N_D q}{2\varepsilon} \left(\frac{W_t}{2}\right)^2 - \frac{N_D q}{2\varepsilon} \left[x_t^2 + x_n^2 + \left(x_t - \frac{W_t}{2}\right)^2\right] + \frac{N_D q}{\varepsilon} \left(x_t - \frac{W_t}{2}\right) x_t + \frac{N_A q}{\varepsilon} x_p x_n + \frac{N_A q}{2\varepsilon} x_p^2 - V.$

To complete the set of equations, it is needed to determine the values of $x_p$, $x_n$ and $W_t$.

$$x_p = \left(\frac{N_D}{N_D + N_A}\right) W \tag{A.1}$$

$$x_n = \left(\frac{N_A}{N_D + N_A}\right) W \tag{A.2}$$

$$W = \sqrt{\frac{2\varepsilon}{q} \left(\frac{N_A + N_D}{N_A N_D}\right) (V_{\text{bi}} + V - 2k_{\text{b}}T)} \tag{A.3}$$

$$W_t = \frac{(N_D + N_t)\, d}{N_D}\,. \tag{A.4}$$

### A.2 One space charge region case

- **Region $P+$, $n$ $-x_L < x < -x_p$**: in this region, silicon is not depleted, and therefore the equations will be:
  - $\varepsilon_{P+,n}(x) = 0$;
  - $\Psi_{P+,n}(x) = -V$.
- **Region $P+$ $-x_p < x < 0$**: in this region, silicon is depleted, and therefore, by solving the Poisson equations:
  - $\varepsilon_{\text{P+}}(x) = -\frac{N_A q}{\varepsilon}(x + x_p)$;
  - $\Psi_{\text{P+}}(x) = \frac{N_A q}{2\varepsilon} \left(x + x_p\right)^2 - V$.
- **Region 1** $0 < x < x_t$: also in this region silicon is depleted, and therefore:
  - $\varepsilon_1(x) = \frac{N_D q}{\varepsilon} x - \frac{N_A q}{\varepsilon} x_p$;
  - $\Psi_1(x) = -\frac{N_D q}{2\varepsilon} x^2 + \frac{N_A q}{\varepsilon} x_p x + \frac{N_A q}{2\varepsilon} x_p^2 - V$.
- **Region 2** $x_t < x < x_n$: Si is not depleted:
  - $\varepsilon_2(x) = \frac{N_D q}{\varepsilon} x - \frac{N_A q}{\varepsilon} x_p - \frac{(N_D + N_t) q}{\varepsilon} d$;
  - $\Psi_2(x) = -\frac{N_D q}{2\varepsilon} x^2 + \left(\frac{N_A q}{\varepsilon} x_p + \frac{(N_D + N_t) q}{\varepsilon} d\right) x + \left\{\frac{(N_D + N_t) q}{\varepsilon} d x_t + \frac{N_A q}{2\varepsilon} x_p^2 - V\right\}$.
- **Region $N-$, $x_n < x < x_R$**: Silicon is not depleted:



2016 JINST 11 P08016

- $\varepsilon_{N-}(x) = 0$;
- $\Psi_{N-}(x) = -\frac{N_D q}{2\varepsilon} x_n^2 + \left(\frac{N_A q}{\varepsilon} x_p + \frac{(N_D+N_t)q}{\varepsilon} d\right) x_n + \left\{\frac{(N_D+N_t)q}{\varepsilon} d x_t + \frac{N_A q}{2\varepsilon} x_p^2 - V\right\}$.

To complete the set of equations, it is needed to determine the values of $x_p$ and $x_n$.

$$x_n = \frac{N_A}{N_D} x_p + \frac{(N_D+N_t)}{N_D} d \tag{A.5}$$

$$x_p = \frac{-\left(\frac{q}{\varepsilon}\frac{N_A(N_D+N_t)}{N_D} d\right) + \sqrt{\left(\frac{q}{\varepsilon}\frac{N_A(N_D+N_t)}{N_D} d\right)^2 - 4\frac{qN_A}{2\varepsilon}\left(\frac{N_A}{N_D}+1\right)\left[\frac{(N_D+N_t)q}{\varepsilon} d\left(\frac{1}{2}\frac{N_D+N_t}{N_D} d - x_t\right) - V_{\text{bi}} - V\right]}}{\frac{qN_A}{\varepsilon}\left(\frac{N_A}{N_D}+1\right)}. \tag{A.6}$$

From equations (A.5) and (A.6), knowing the full depletion voltage $V_{\text{fd}}$ and the length of the bulk $x_R$, and that at full depletion $x_n = x_R$, it is possible to extract the charged traps volume density $N_t$. The set of equations (A.7), (A.8), (A.9) and (A.10) shows the relations that link $N_t$ to $V_{\text{fd}}$.

$$a_{N_t} = \left(\frac{qN_D}{\varepsilon}\right)^2 \left(1 + \frac{N_A}{N_D}\right) \tag{A.7}$$

$$b_{N_t} = \left(\frac{qN_D}{\varepsilon}\right)^2 \left(\frac{N_A}{N_D} + 1\right) x_R + \frac{q^2 N_A}{\varepsilon^2} x_t (N_A + N_D) \tag{A.8}$$

$$c_{N_t} = \left(x_R \frac{qN_D}{\varepsilon}\left(\frac{N_A}{N_D} + 1\right)\right)^2 - 2(V_{\text{bi}} + V_{\text{fd}}) \frac{qN_A}{\varepsilon}\left(\frac{N_A}{N_D} + 1\right) \tag{A.9}$$

$$N_t = N_D \left(\frac{b_{N_t} - \sqrt{b_{N_t}^2 - a_{N_t} * c_{N_t}}}{d * a_{N_t}} - 1\right) \cong N_D \frac{b_{N_t} - \sqrt{b_{N_t}^2 - a_{N_t} * c_{N_t}}}{d * a_{N_t}}. \tag{A.10}$$

## B Equations of motion of electrons

In this appendix, the solutions of the differential equation (3.11) are shown, for each region of the diode, in the one space charge region case (in the case with two space charge regions, it is possible to consider equations until Region 1, until time $t_n$, that is the time for which $r(t_n) = x_n$).

The notation $W(x)$ refers to the Lambert W function of $x$.

- **Region $P+$ $\quad -x_p < x < 0$**

$$r = -x_p + EW\left(\frac{1}{\mathrm{E}} e^{\frac{v_{\text{sat}} t + K_{0b}}{\mathrm{E}}}\right) + K_{0_a} \tag{B.1}$$

where:

$$K_{0,b} = E \ln(-K_{0,a}) - K_{0,a} \tag{B.2}$$

$$K_{0,a} = -1 \tag{B.3}$$

$$E = \frac{\varepsilon}{\mu_{e_0} N_A q} v_{\text{sat}} \tag{B.4}$$



2016 JINST 11 P08016

and $\varepsilon$ is the silicon permittivity, $\mu_{e_0}$ is the electrons mobility at low electric field, $N_A$ is the doping concentration of the P+ region, $q$ is the electron charge and $v_{\text{sat}}$ is the saturation velocity, given by equation

$$v_{\text{sat}} = v_{\text{sat},0} \left( \frac{300K}{T} \right)^{0.87} \tag{B.5}$$

where $v_{\text{sat},0} = 1.07 \times 10^7 cm/s$.

- **Region 1 $\mathbf{0 < x < x_t}$**

  At time $t_1$, the middle of the electrons cloud will reach the position 0.

$$t_1 = \frac{x_p + E \ln\left(\frac{K_{0,a} - x_p}{K_{0,a}}\right)}{v_{\text{sat}}} \tag{B.6}$$

$$K_1 = \frac{N_A}{N_D} x_p + E_1 \ln\left(\frac{N_A}{N_D} x_p\right) + v_{\text{sat}} t_1 \tag{B.7}$$

$$r = \frac{N_A}{N_D} x_p - E_1 W\left(\frac{1}{E_1} e^{\frac{-v_{\text{sat}} t + K_1}{E_1}}\right) \tag{B.8}$$

  where

$$E_1 = \frac{v_{\text{sat}} \varepsilon}{N_D q \mu_{e_0}} \tag{B.9}$$

  and $N_D$ is the doping concentration of the N- region. The middle of the electrons cloud will reach the position $x_n$, in case of two separated depletion regions, at time $t_n$.

$$t_n = \frac{-x_n + \frac{N_A}{N_D} x_p + E_1 \ln\left(-x_n + \frac{N_A}{N_D} x_p\right) - K_1}{-v_{\text{sat}}}$$

  since in the case of two separated depletion regions the electric fields vanishes at $x_n$, $t_n = +\infty$.

- **Region 2 $\mathbf{x_t < x < x_n}$**

  At time $t_2$, the middle of the electrons clouds will reach the position $x_t$.

$$t_2 = \frac{-x_t + \frac{N_A}{N_D} x_p + E_1 \ln\left(-x_t + \frac{N_A}{N_D} x_p\right) - K_1}{-v_{\text{sat}}} \tag{B.10}$$

$$K_2 = -x_t + \frac{N_A}{N_D} x_p + \frac{(N_D + N_t)}{N_D} d + E_1 \ln\left(-x_t + \frac{N_A}{N_D} x_p + \frac{(N_D + N_t)}{N_D} d\right) + v_{\text{sat}} t_2 \tag{B.11}$$

$$r = \frac{N_A}{N_D} x_p + \frac{(N_D + N_t)}{N_D} d - E_1 W\left(\frac{1}{E_1} e^{\frac{-v_{\text{sat}} t + K_2}{E_1}}\right). \tag{B.12}$$

## References


[1] N. Wermes, *Pixel detectors for particle physics and imaging, applications*, *Nucl. Instrum. Methods Phys. Res. Sect.* **A 512** (2003) 277.

[2] N. Wermes, *Pixel detectors for tracking and their spin-off in imaging applications*, *Nucl. Instrum. Methods Phys. Res. Sect.* **A 541** (2005) 150.




2016 JINST 11 P08016

[3] L. Rossi, P. Fischer, T. Rohe and N. Wermes, *Pixel Detectors. From Fundamentals to Applications*, Springer-Verlag Berlin Heidelberg (2006).

[4] W. Snoeys, *Monolithic pixel detectors for high energy physics*, *Nucl. Instrum. Methods Phys. Res. Sect.* **A 731** (2013) 125.

[5] C. Flötgen, N. Razek, V. Dragoi and M. Wimplinger, *Novel Surface Preparation Methods for Covalent and Conductive Bonded Interfaces Fabrication*, *ECS Trans.* **64** (2014) 103.

[6] J. Burggraf, J. Bravin, H. Wiesbauer and V. Dragoi, *Monolithic thin wafer stacking using low temperture direct bonding*, *ECS Trans.* **64** (2014) 95.

[7] V. Eremin, N. Strokan, E. Verbitskaya and Z. Li, *Development of transient current and charge techniques for the measurement of effective net concentration of ionized charges ($N_{\rm eff}$) in the space charge region of p-n junction detectors*, *Nucl. Instrum. Methods Phys. Res. Sect.* **A 372** (1996) 388.

[8] V. Eremin, E. Verbitskaya and Z. Li, *The origin of double peak electric field distribution in heavily irradiated silicon detectors*, *Nucl. Instrum. Methods Phys. Res. Sect.* **A 476** (2002) 556.

[9] G. Kramberger et al., *Investigation of irradiated silicon detectors by edge-TCT*, *IEEE Trans. Nucl. Sci.* **57** (2010) 2294.

[10] M.F. García et al., *High-resolution three-dimensional imaging of a depleted CMOS sensor using an edge Transient Current Technique based on the Two Photon Absorption process (TPA-eTCT)*, in press [*Nucl. Instrum. Methods Phys. Res. Sect.* (2016)].

[11] Synopsys, *TCAD Sentaurus*, version I–2013.12 (2013).

[12] W.R. Fahrner and S. Löffler, *Determination of the Trap Density in Amorphous Silicon by Quasi-Static Capacitance-Voltage Measurements*, *J. Electrochem. Soc.* **145** (1998) 1786.

[13] S.M. Sze, *Physics of Semiconductor Devices*, John Wiley & Sons (1981).

[14] R. Eber, *Investigations of new Sensor Designs and Development of an effective Radiation Damage Model for the Simulation of highly irradiated Silicon Particle Detectors*, Ph.D. Thesis, KIT, Karlsruhe Germany (2013), p. 150 [IEKP-KA/2013-27].

[15] J. Fink, H. Krüger, P. Lodomez and N. Wermes, *Characterization of charge collection in CdTe and CZT using the transient current technique*, *Nucl. Instrum. Methods Phys. Res. Sect.* **A 560** (2006) 435.

[16] M. Moll, *Radiation Damage in Silicon Detectors*, Ph.D. Thesis, Universität Hamburg, Hamburg Germany (1999), p. 251 and online pdf version at https://mmoll.web.cern.ch/mmoll/thesis/pdf/moll-thesis.pdf.

[17] W. Shockley and W.T. Read, *Statistics of the Recombination of Holes and Electrons*, *Phys. Rev.* **87** (1952) 835.

[18] G. Lutz, *Effects of deep level defects in semiconductor detectors*, *Nucl. Instrum. Methods Phys. Res. Sect.* **A 377** (1996) 234.

[19] G. Sasso, N. Rinaldi, G. Matz and C. Jungemann, *Analytical models of effective DOS, saturation velocity and high-field mobility for SiGe HBTs numerical simulation*, in *International Conference on Simulation of Semiconductor Processes and Devices*, IEEE (2010), p. 279.

[20] S.M. Sze, *Basic equations for semiconductor-device operation*, in *Physics of Semiconductor Devices*, 2nd edition, section 1.7, Wiley (1981), pp. 50–57.

[21] A.G. Bates and M. Moll, *A comparison between irradiated magnetic Czochralski and float zone silicon detectors using the transient current technique*, *Nucl. Instrum. Methods Phys. Res. Sect.* **A 555** (2005) 113.

2016 JINST 11 P08016